Simulation of steep waves interacting with a cylinder by coupling CFD and Lagrangian models

Pablo Higuera[1], *Eugeny Buldakov*[2] *and Dimitris Stagonas*[3]
[1]University of Auckland, Department of Civil and Environmental Engineering, Private Bag 92019, Auckland, New Zealand
[2]University College London, Department of Civil Engineering, London, UK
[3]Department of Civil and Environmental Engineering, University of Cyprus, Nicosia, Cyprus

ABSTRACT

This paper presents numerical modelling results of the interaction between a group of steep waves and a fixed vertical cylinder performed with a one-way coupled hybrid model. A set of experimental data is used to benchmark the accuracy of the modelling results. The wavemaker signal generated in the physical experiments is used to reproduce the incident wave conditions without a priori knowledge of the rest of the dataset. A Lagrangian numerical wave flume propagates the wave group, producing the non-linear free surface elevation and wave kinematics with high accuracy in the vicinity of the cylindrical structure. This data is used as the input to the *olaFlow* CFD model, which calculates the wave-structure interactions. One-way coupling approaches based on boundary conditions and relaxation zones are tested and compared in terms of the recorded free surface elevation and pressures at the structure. Results present an adequate degree of accordance and turbulence effects are found to be negligible in the simulations.

KEY WORDS: Wave-structure interaction; cylinder; Lagrangian wave model; *olaFlow*; OpenFOAM.

INTRODUCTION

Wave and structure interaction (WSI) is a field in which numerical modelling is being applied consistently and with increasing popularity. The challenges derived from modelling the impact of waves and structures are numerous. Marine and offshore structures are usually located in areas subjected to extremely harsh conditions, in which often waves present three-dimensional and highly-nonlinear processes such as wave breaking and wave impacts may result in impulsive loading.

Under such conditions the relevance of numerical modelling, and especially computational fluid dynamics (CFD), derives from the low number of underlying assumptions that the Navier-Stokes equations involve, from their inherent nonlinearity and from their capability to include turbulence dissipation effects via Reynolds-Averaged Navier-Stokes (RANS) or Large Eddy Simulation (LES) turbulence models. Furthermore, despite its advantages and flexibility, numerical modelling results alone have a limited practical credibility if they are not accompanied by a reasonable validation against experimental measurements, which is why physical and numerical modelling should be deemed as complementary approaches.

Another of the limitations of CFD is the large computational cost required, which makes them an impractical approach to simulate extensive domains and long time series. Instead, hybrid modelling (HM) appears to be gaining momentum to reduce such limitations. The concept behind HM consists in simulating the different areas of interest with several numerical techniques, according to the complexity of the processes occurring within each one. For example, under certain circumstances wave propagation can be accurately simulated with a potential flow theory model instead of using CFD, thus saving a significant amount of computational resources and time. The potential flow theory modelling may be performed until close to the structure of interest, where the CFD model calculations would take over to simulate the detailed interactions (e.g. Lachaume et al. (2003); Kim et al. (2010); Guo et al. (2012)).

There are two principal approaches to link the numerical models. In one-way coupling, one of the models is run first independently from the other and the data is passed to the second one, so there is no connection of feedback loop between both models. In two-way coupling, both models are run concurrently and they exchange information at the interface (which can be a boundary or a region in space). This way, waves could ideally propagate across models seamlessly. Despite being a more complete and realistic approach, two-way coupling models present significant technical and numerical implementation challenges, for example, in terms of blending solutions from two sets of equations.

In this paper we introduce a one-way coupling HM approach between a Lagangian and CFD models. The Lagrangian model propagates the wave group and generates the dataset of wave kinematics to feed the CFD model using the displacement of the physical wavemaker as only input. Then the CFD model reproduces the incident wave conditions via a boundary condition and a relaxation zone without additional tuning.

This paper is structured as follows. The physical experiments are described after this introductory chapter. The Lagrangian model is introduced next, and the wave propagation simulations are validated. Afterwards, the CFD model is described, along with the different setups tested in two- and three-dimensions. Then, the comparison between the CFD modelling and the experiments are analysed. Finally, the conclusions and future work are drawn.

PHYSICAL EXPERIMENTS SETUP

The experiments reproduced in this paper were performed in a flume (110 x 2.2 x 2.0 m) at the Franzius-Institute Laboratory in Hannover. The description of the flume and methodology of wave generation used in the experiments can be found in Sriram et al. (2020). The setup consisted in an instrumented fixed cylinder (0.22 m of diameter) subjected to the impact of focussed wave groups. The cylinder centre was located 24.88 m from the wavemaker ($x = 0$) and 1.085 m from the sidewall of the flume, slightly off-center by 2.5 cm. This deviation has been deemed small enough as compared to the total width of the flume (2.2 m) to consider the case symmetric when later reproducing it numerically.

The wave conditions reproduced in this work (cases 23001 and 23003) correspond to uni-directional focused wave groups with a constant steepness spectrum, created by 32 components with frequencies between 0.34 Hz an 1.02 Hz, and amplitudes of 5 and 20 cm. The nominal focusing distance is $x = 23$ m for a working water depth of 0.7 m. The focused waves were generated by a hydraulic piston wavemaker using the second order correction technique introduced in Schäffer (1993). The wavemaker displacement time series, the free surface elevation (FSE) at 7 locations along the flume and 8 pressure probes measurements mounted on the cylinder (see positions in Table 1) have been reported at 100 Hz.

Table 1 Location of the free surface elevation and pressure probes. x measured from the wavemaker; y measured from the flume centreline; z measured from the bottom of the flume; β measured from the negative x direction. Distances in m.

	WP1	WP2	WP3	WP4	WP5	WP6	WP7
x	4.975	13.928	14.178	14.428	24.31	24.88	25.585
y	0	0	0	0	0.275	0.275	0.275
	PP1	PP2	PP3	PP4	PP5	PP6	PP7	PP8
z	0.415	0.515	0.615	0.715	0.815	0.615	0.615	0.615
β	0°	0°	0°	0°	0°	20°	90°	180°

INCOMING WAVE CONDITIONS

In this work we use a Lagrangian Numerical Wave Tank (LNWT), also previously used in Higuera et al. (2018), as a fast component of the hybrid model to reconstruct the incoming wave conditions. The LNWT solves the Lagrangian continuity and vorticity conservation equations for inviscid fluids and the dynamic free surface condition. Full details can be found in Buldakov et al. (2019).

The LNWT has been used to replicate the wave flume where the experimental dataset was generated. The two-dimensional rectangular Lagrangian computational domain has a depth of 0.7 m and a length of 60 m. The Lagrangian model is expected to reproduce the wave behaviour before the cylinder position ($x \approx 25$ m), therefore, the length of the computational domain is much shorter than the length of the experimental tank (110 m). Moreover, since the Lagrangian modelling is 2D, the cylinder has not been reproduced.

A piston-type wavemaker has been modelled as a vertical wall moving with a prescribed displacement starting from the initial position ($x = 0$). The incoming wave for the experimental case was generated using the actual motion of the experimental wave paddle provided. Unlike the cases presented in Higuera et al. (2018), in which no experimental wave generator movement was available, wave generation was straightforward in this work and no iteration procedure was required. A dissipative region has been implemented between $x = 40$ m and $x = 60$ m to reduce reflections from the far end of the LNWT, where an impenetrability (slip) boundary condition is applied on the vertical end wall.

The computational parameters of the Lagrangian model have been selected as the result of a convergence test for case 23003. The computations were carried out as the combination of three sizes of computational mesh 401×11, 601×11 and 801×11, and two time steps 0.004 s and 0.002 s. The FSE was sampled at selected locations corresponding to the positions of experimental wave probes (Table 1). The differences between the wave profiles far from the wave maker (WP7) were found negligible for both time steps and for the two largest horizontal mesh resolutions.

Buldakov et al. (2019) showed that the vertical mesh resolution has little effect on the FSE profile, but can have a significant impact on wave-generated velocities. The convergence of velocity profiles for increased vertical mesh resolution was checked by an additional case with a 601×16 mesh and 0.004 s time step. Slight differences between the wave profiles calculated with different vertical resolutions were observed, therefore, we selected the case with 601×16 mesh and 0.004 s time step as the main computational case. The computational time for modelling 60 s of wave evolution in serial with the selected mesh and time step was approximately 20 hours.

It should be noted that due to the implicit time marching scheme used by the Lagrangian solver the computational time grows rapidly with increasing mesh sizes, and in this work the computational parameters are chosen to provide the optimum quality for wave kinematics. If the computational time was a limiting criterion, a case with a 601×11 mesh would still provide an acceptable accuracy with considerably lower computation time (6 hours on a single processor for a 60 s run). For future works, improving the computational efficiency of the Lagrangian solver may be achieved as discussed in Buldakov et al. (2019).

As shown in Figure 1, the LNWT reproduces the experimental FSE with an acceptable accuracy in both cases. Slight discrepancies could be caused by the reflection of the waves at the cylinder during the experiment and by the reflections of long wave components not fully absorbed by the dissipative region at the far end of the LNWT.

Wave kinematics (FSE and velocities) calculated by the LNWT have been extracted between $x = 20$ m and $x = 20.2$ m for 2D simulations and between $x = 23$ m and $x = 23.2$ m for the 3D simulations, to be used for the wave generation condition for the CFD model.

CFD MODEL AND SETUP

The CFD solver *olaFlow* (Higuera et al., 2013; Higuera, 2017), developed with the OpenFOAM® (Weller et al., 1998) library has been applied in this work. *olaFlow* is a numerical model highly specialized in the simulation of waves and wave-structure interaction, solving the

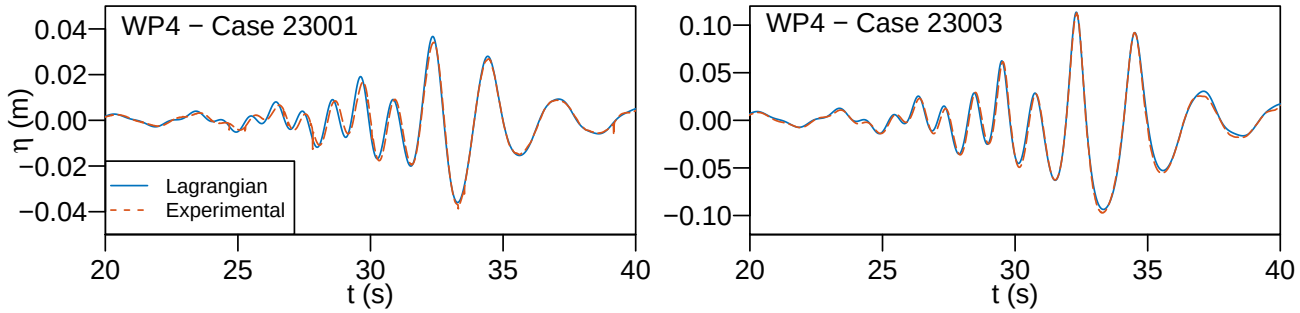

Fig. 1 Comparison of surface elevation of the experimental incoming wave at x = 14.428 m (WP4) with calculations by the Lagrangian model.

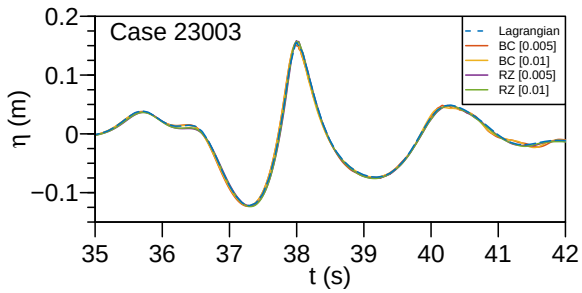

Fig. 2 Preliminary comparison of FSE between the Lagrangian and the 2D CFD simulations at x = 23 m. Cell resolution given in m.

Reynolds-Averaged Navier-Stokes equations for two phases (water and air). The incompressible continuity and Navier-Stokes equations are:

$$\frac{\partial \rho}{\partial t} + \nabla \cdot (\rho \, \mathbf{U}) = \mathbf{0}, \tag{1}$$

$$\frac{\partial \rho \mathbf{U}}{\partial t} + \nabla \cdot (\rho \mathbf{U}\mathbf{U}) = -\nabla p^* - \mathbf{g} \cdot \mathbf{r} \, \nabla \rho + \nabla \cdot (\mu_{\mathbf{eff}} \nabla \mathbf{U}) + \sigma \kappa \nabla \alpha, \tag{2}$$

in which ρ is the density, $\mathbf{U}$ is the velocity vector, t is time and ∇ is the gradient operator. The dynamic pressure (p^*) is derived from total pressure (p) by the expression $p^* = p - \rho \mathbf{g} \cdot \mathbf{r}$, in which $\mathbf{g}$ is the acceleration due to gravity and $\mathbf{r}$ is the position vector, see Márquez (2013) for further reference. The fluid viscosity is included in the equations, where μ_{eff} represents the effective dynamic viscosity, comprising the molecular and turbulent components. The last term introduces the surface tension force, where σ is the surface tension coefficient; κ is the curvature of the free surface.

In the algebraic Volume of Fluid (VOF) technique (Berberovic et al., 2009) applied the indicator function (α) tracks the amount of water per unit volume in the mesh cells and the flow phases are advected following:

$$\frac{\partial \alpha}{\partial t} + \nabla \cdot (\alpha \mathbf{U}) + \nabla \cdot [\alpha(\mathbf{1} - \alpha)\mathbf{U_c}] = \mathbf{0}, \tag{3}$$

where $\mathbf{U_c}$ is a numerical compression velocity (calculated automatically in OpenFOAM® with a compression factor $c_\alpha = 1$) to prevent the diffusion of the air-water interface. For further information the reader is referred to Higuera (2015).

The implementation of the one-way coupling interface between the Lagrangian model and *olaFlow* is either via a fixed-value boundary condition (BC) or a relaxation zone (RZ). The coupling BC has been previously reported in Higuera et al. (2018) and has been updated to be linked with active wave absorption (Higuera, 2020). This procedure allows dissipating the waves incident to the boundary (e.g. reflections on the cylinder) while still generating the target wave conditions.

Relaxation zones are an alternative one-way coupling procedure newly-introduced in this work. A RZ is a volume in which the Lagrangian model kinematics (FSE and velocities) and the Navier-Stokes equations solution are blended progressively. The main advantages of RZs are that they allow generating steeper waves without premature breaking at the wave generation boundary (although this is not an issue in the present simulations) and, most importantly, generating outbound and absorbing incoming waves (i.e., reflected from the cylinder) simultaneously. The RZ formulation chosen in this work is the same previously applied in Higuera (2020), and introduced in Fuhrman et al. (2006); Jacobsen et al. (2012), which uses the equations:

$$\Lambda = w_R \, \Lambda_{\mathrm{NS}} + (1 - w_R) \, \Lambda_{\mathrm{LA}} \tag{4}$$

$$w_R = 1 - \frac{e^{\sigma^P} - 1}{e - 1} \tag{5}$$

to relax the VOF (α) and velocities ($\mathbf{U}$) explicitly after solving the VOF advection equation and before solving the pressure Poisson equation. Here, Λ is the variable of interest and the subscripts *NS* and *LA* indicate the Navier-Stokes solution and the Lagrangian model values at each cell. The variable w_R is the blending function (weight), which varies smoothly between 0 and 1 within the RZ, and σ is a local coordinate system so that $w_R(\sigma = 0) = 1$ at the interface between the RZ and the inner domain of the simulation and $w_R(\sigma = 1) = 0$ at the wave generation/absorption boundary. The parameter P value defines the shape of the relaxation function. In this case a value of $P = 3.5$ has been chosen, as advised in Jacobsen et al. (2012).

Unlike the BC, which only needs the kinematics' values at a single location, the RZ requires data over the whole area at each time step to generate waves. This multiplies the amount of input data from the wave propagation model that needs to be stored, especially if high resolution in time is required. Generally the wave generation/absorption performance of RZs is dependent on their length, being a length of approximately one wavelength advised to absorb waves effectively Fuhrman et al. (2006). However, the longer the RZ, the higher computational cost it bears, therefore, a balance between both needed to be found, as explained next.

The input data used in the RZ has 3 dimensions, 2 in space (x and z) and time, and is discrete, therefore it needs to be interpolated to each of the cells inside the RZ every time step. The procedure involves 3 linear interpolation steps. Initially, linear interpolation is performed in the z direction for the closest neighbors in x and t among the data available (4 operations). Then, linear interpolation is per-

formed in time (2 operations) and finally in the x direction (2 operations).

Another novelty of this work is that the BC and RZ have been updated to accept non-uniform time series. The data from the LNWT is stored with larger time steps (0.1 s) during times of small free surface elevation variations and smaller time steps (0.01 s) for steeper waves. This procedure ensures that the wave crests and troughs are generated more accurately, avoiding trimming them as a result of interpolation in time, while minimising the amount of input data needed to run the CFD case.

The CFD modelling simulations involved two stages, neither of which required any kind of tuning or adjustments. In the first stage the initial validation of the RZ and BC and mesh convergence study were performed in 2D. The 2D mesh was simple, structured and conformal, formed by hexahedral cells. The wave generation boundary (i.e. interface with the Lagrangian model) was located at x = 20 m and the cells in the vicinity of that area were 0.5 cm long in the horizontal direction. Starting from x = 25.6 m, the cell size in the wave propagation direction (x) started growing progressively until 0.5 m at the opposite end of the flume, located 30 m away. This long distance was chosen to delay any possible reflections from the end boundary while the very coarse mesh gradation is commonly applied to dissipate wave energy numerically (Skene et al., 2018) while noticeably reducing the computational cost (as compared to using the smaller cell size everywhere). The mesh was 1.1 m in the vertical direction, with vertical cell sizes varying from 1 cm to 0.5 cm from z = 0 to z = 0.5 m and from 0.5 cm to 1 cm from z = 0.9 m to z = 1.1 m, over the entire length of the flume. A mesh with half the resolution was also tested, finding no significant differences.

Regarding BCs, the bottom is a wall condition (no-slip) while the top BC corresponds to atmospheric pressure. The lateral walls impose the desired 2D behaviour with a free-slip BC. The Courant number was set to 0.25 in all simulations, a value that has been found low enough to provide a reasonable accuracy while keeping a good balance with the computational time required to simulate the case. The 2D fine mesh totals 250,000 cells and a single case of 50 s is completed in parallel with 4 cores (Intel Xeon Gold 6138, 2.0 GHz) in 35 minutes.

Waves were generated with the coupling BC at the leftmost boundary (x = 20 m) and absorbed with active wave absorption at the opposite end in one of the alternatives. This case has also been run with RZs. Two different wave generation RZ which span for 20 cm (i.e. 40 cells for the fine mesh) and 30 cm were tested, with virtually the same results, while an additional RZ of 20 m was placed at the opposite end for wave absorption. The input data from the LNWT was provided with a constant discretization in the x direction of 0.5 cm and 1 cm, again with no significant changes in the results, while 16 points with varying z locations depending on the local FSE were given; time intervals were between 0.1 s and 0.01 s, as previously reported.

The comparisons between the 2D CFD and the LNWT FSE bear a high degree of accordance at the theoretical focussing point (x = 23 m), as shown in Figure 2. The results indicate that both the BC and RZ couplings produce very accurate results, with minor differences between them. For example the BC simulation produces a slightly better wave shape before the focussing event (t = 36.4 s), whereas the accordance of RZ simulations is slightly better after focussing (t = 41.4 s), probably due to the higher degree of absorption of the RZ at the end of the flume.

The lessons learnt with these initial 2D simulations were applied to design the latter 3D mesh and case. The excellent results conveyed that the relaxation zone length of 20 cm, the input data at 1 cm intervals and sampling rate were appropriate for these particular conditions. However, we also observed that the computational times increase approximately by 5% to 20% when including RZs in the simulations, depending on their extent. Since accurate FSE results were obtained just 3 m away from the wave generation boundary, and even closer to it, the 3D mesh will start at x = 23 m to reduce the computational cost by avoiding to simulate 3 additional metres. Moreover, since the 1 cm resolution has proven to be sufficiently accurate, 3D mesh will use such cell size. Finally, despite the fact that the BC simulation configuration is more computationally efficient and shows a slightly higher fidelity prior to the focussing event, both the BC and RZ techniques will be tested.

The 3D mesh has been designed to be a high quality structured cylinder-fit mesh. The sketch of the mesh (top view) showing all the different blocks (red lines) used is presented in Figure 3. The overall length of the mesh is reduced with respect to the 2D case (x = 23 m to x = 45 m) and the vertical dimension was set to 1.1 m. The 3D mesh is 1.1 m in the spanwise direction too (y = 0 m - y = 1.1 m), which corresponds to half of the domain of the physical flume. This reduces the computational costs by half assuming an overall symmetric behaviour of the case.

The general cell size is approximately 1 cm in all three directions and due to the geometry of the blocks it gets reduced to 1.5-1.8 mm in the horizontal directions near the cylinder wall, while the vertical cell size remains constant everywhere and equal to 1 cm. As observed in Figure 3 certain areas closer to the lateral wall (e.g. top left corner), which are relatively far from the area of interest, present noticeably larger cell sizes in the horizontal directions. The cell size in the x direction also grows larger, up to 25 cm, near the wave absorption boundary (x = 45 m) to reduce the total number of cells.

The BCs are the same as in the 2D case, save the lateral boundaries, one of which is a symmetry plane. The boundary opposite to it and the cylinder surface are both walls (no-slip BC). Turbulent effects are expected to be limited, therefore, all the cases have been deemed as laminar. Nevertheless, the 3D case has also been run with the SST k-ω turbulence model (Devolder et al., 2017). The numerical setup for the turbulent variables is the same as in Devolder et al. (2017).

The 3D mesh totals 7 million cells and each case of 50 s is completed in parallel with 72 cores in approximately 35 hours, therefore, the complete hybrid modelling (LNWT plus CFD) took 55 hours.

RESULTS

The results from the free surface elevation (WP5-WP7) and pressure gauges mounted on the cylinder surface (Table 1) for cases 23001 and 23003 (cases 1 and 3, for short) are analysed in this section. Waves have been generated with the BC technique in the cases *BC* and *SST*, and with the RZ technique in case *RZ*. Furthermore, cases *BC* and *RZ* are laminar, while case *SST* uses the SST k-ω turbulence model.

Figures 4 and 5 show the FSE elevation comparisons for gauges WP5-WP7 during the focussing event for cases 1 and 3. The location of the gauges relative to the cylinder can be observed in Figure 3. Overall the degree of accordance between the experimental and numerical results is appropriate and there are no evident discrepancies between the BC and RZ approaches. Nevertheless, modelling seems to overestimate the peak wave heights in case 1 by approximately 7.5%, while the troughs are more accurately captured.

WP5 is located 1.31 m after the theoretical focussing location, and

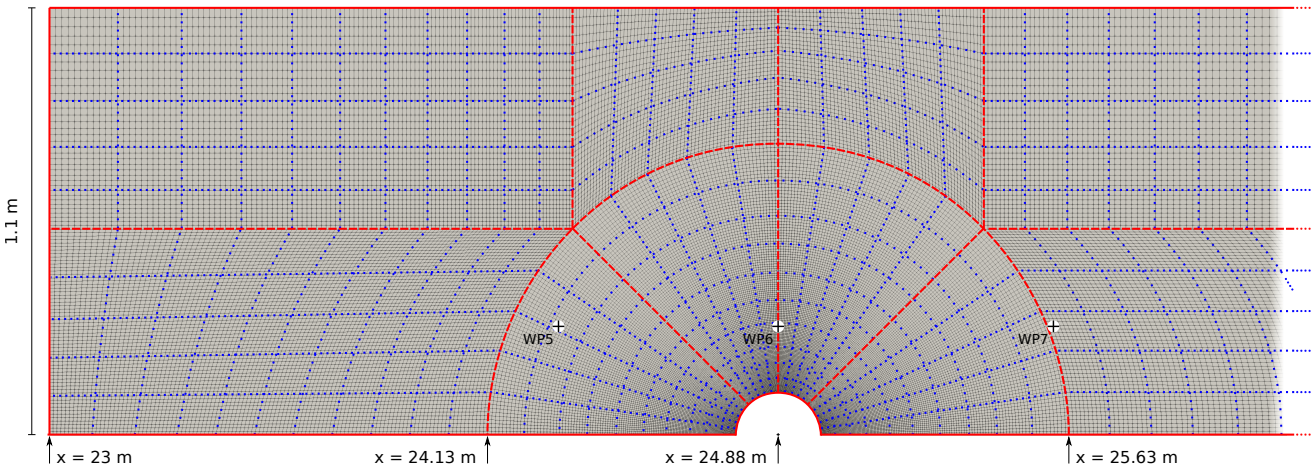

Fig. 3 *olaFlow* numerical mesh (top view). The mesh cells are plotted in black and the individual blocks of the mesh are outlined in red lines. Since cells might not be visible at certain locations due to image resolution, blue dotted lines indicate the internal structure of such blocks. The location of free surface elevation probes WP5-WP7 is included in the sketch.

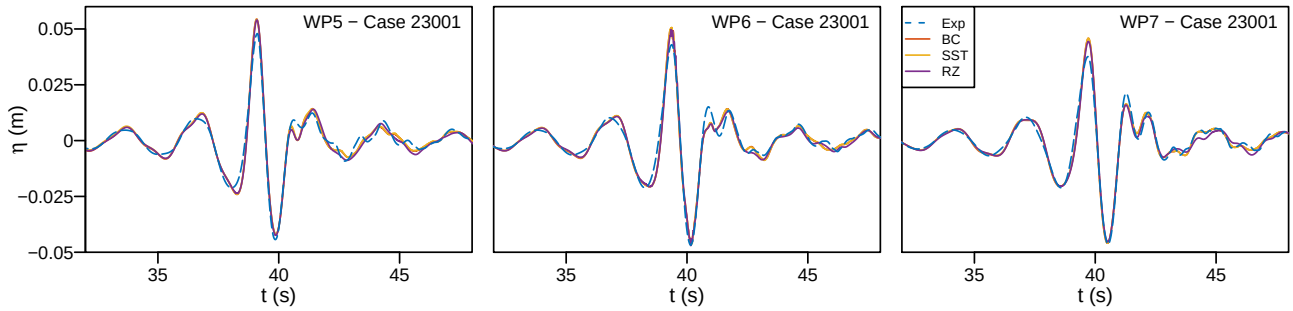

Fig. 4 Comparison of FSE time series between the experiments and the CFD simulations at gauges WP5-WP7. Case 23001.

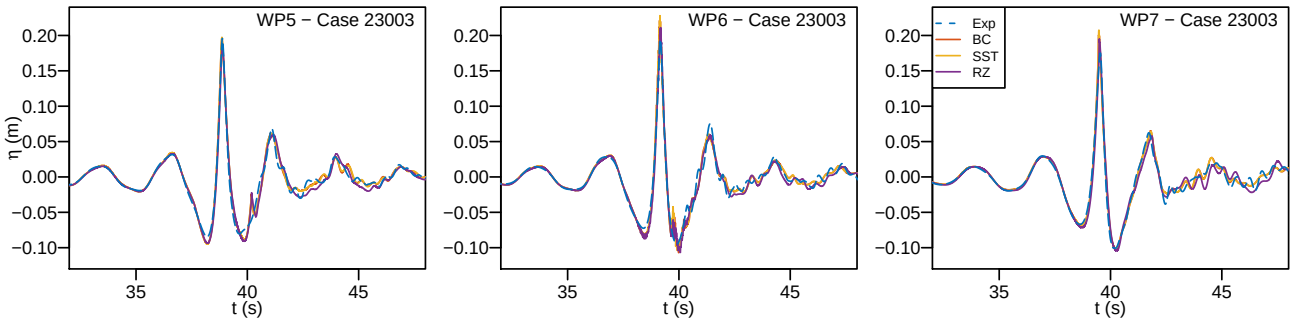

Fig. 5 Comparison of FSE time series between the experiments and the CFD simulations at gauges WP5-WP7. Case 23003.

presents the best results in terms of matching the amplitude of the focussed wave in case 3, so we will use it as a benchmark. Both BC simulations, for the laminar and SST k-ω turbulence model, capture the crest peak within an accuracy of 1.6 mm while the RZ simulation is 8.5 mm below and, thus, the peak lags 0.02 s behind. The wave troughs right before and after the main wave are overestimated by 10 and 8 mm, respectively, which produces a noticeable difference in the wave shape, namely with a steeper front and a milder tail. The agreement at those troughs gets better approaching WP7 for all cases.

Another discrepancy can be noticed at t = 40.2 s in WP5-6 case 3, when a steep wave front appears in all the numerical simulations, but not in the experimental data. This is caused by the wave that is radiated at the cylinder, which propagates back after rundown. High frequency oscillations on top of the incoming waves can be observed after t = 41.7 s due to the reflections on the lateral boundaries, which are also noticeable in the experiments. Since the wave height is much lower in case 1, the oscillations are also smaller, therefore the model fails to capture them, probably because of a lack of high enough resolution.

The results at WP6 and WP7, which are located side by side in line with the centre of the cylinder and 0.7 m seaward from the cylinder are

very similar. The troughs are still underestimated by approximately 1 cm in case 3 and better captured in case 1, but the main wave crest is significantly overestimated in all cases. For example, by 1.6 cm (RZ) and 3.3 cm (BC) at WP6 case 3. Additional 3D simulations performed with the inlet boundary at $x = 20$ m (3 m seaward with respect to the results shown) did not present significant improvements at WP5-WP6, indicating that the mismatch at those gauges is not caused by boundary effects because of the proximity of the wave generation boundary/RZ.

Figures 6 and 7 show the pressure comparisons for probes PP1-PP8 during the focussing event for cases 1 and 3. It is noteworthy that no experimental data was provided for gauge PP1. Some moderate pressure oscillations (e.g., see PP1 at $t \approx 35$ s) appear in the numerical solutions due to small pressure instabilities arising from solving the pressure Poisson equation iteratively. These fluctuations appear in the figure because numerical data is reported at each time step, which is variable but typically on the order of 0.0005 s (≈2,000 Hz sampling rate), whereas the experimental results were provided at 100 Hz and/or may have been filtered. Generally, no significant differences can be found between all three numerical setups, except for the differences in the amplitude of the largest peak and in the latter stages ($t > 41$ s), when diffracted and reflected waves start to interact. Since the wave troughs were overestimated for case 1 and underestimated for case 3 in terms of FSE in WP5-6, this is also the case for the numerically simulated pressures (e.g. PP2, PP3). Another interesting trend in case 3 is that the main pressure peaks are lower for the RZ case and higher for the BC cases, with the experimental pressure usually lying between the RZ and BC cases values (e.g. PP2-PP5) with deviations of approximately 50 Pa between them. There are some gauges that are initially outside the water and measure pressure only when the FSE is higher during the course of the simulation. For example PP4 successfully captures the timing and magnitude of 4 events in case 3, but it shows a 33% overestimation in case 1, probably due to the lower relative resolution when discretising the smallest wave height. PP5 also starts being emerged and case 3 simulations captures the single peak that reaches it extremely well, whereas in case 1 water does not reach that high, therefore we can only observe a flat line. The shape of the wave in PP7 is very particular, especially for case 3, with flat crest and troughs because the gauge is mounted at 90° with respect to the wave propagation direction. Finally, it can be concluded that the overall degree of accordance for pressure time series in both cases is higher than for FSE.

Figure 8 shows a snapshot of the 3D CFD simulation of case 3 with several different views of the focussed wave during the impact on the cylinder, which permit observing the 3D flow features. The bottom panel shows that the wave crest has just surpassed the cylinder and the water is wrapping around its surface and creating an enhanced runup at the back where the diffracted wave components meet. At this instant ($t = 39$ s) a significant amount of water is still visible at the front part of the cylinder and small ripple-like oscillations on the water surface can be observed around the cylinder (top left panel). These are most likely numerically-induced and caused by a combination of the VOF advection scheme. One reason may be that the main direction of wave propagation differs significantly from the normal directions to the vertical faces on the cells, which are radially-oriented at the area, whereas wave propagates in the positive x direction. This phenomenon is often observed for tetrahedral meshes too. Another factor that can contribute to the small ripples is spurious currents (Wroniszewski et al., 2014). Spurious currents are large and nonphysical velocities that appear at the interface between water and air. In this case the VOF function used is algebraic, therefore, there is no clear distinction or sharp edge between both fluids; instead, they are treated as a continuous mixture governed by Eq. 3. The lack of a "jump condition" at the interface and the large density ratio in such a limited distance (~4 cells) produces these large velocities that can contribute to create the oscillations observed.

Another discrepancy with the experimental observations is the absence of water droplets during the impact, which can be explained by several factors. The most obvious is that the mesh resolution is not fine enough to capture the very small water droplets or spray that are produced by wave impacts. Resolving such complex phenomenon will most likely require sub-millimetric cell sizes to resolve the physics at such small scales. On top of that, cell sizes in the horizontal directions at the vicinity of the cylinder are significantly finer than those in the vertical direction, approximately by a factor of 1:6. This cell aspect ratio eases the advection in the vertical direction and the vertical resolution of 1 cm does not allow the water to form the droplets. A square or more modes aspect ratio (1:2) would be preferred at this area. However, such high resolution will increase significantly the cell number and the computational resources and time needed to run the simulation. Furthermore, a non-conformal mesh could have been adopted instead, however, when the air-water interface goes through a non-conformal area (i.e. where one cell splits into two) it experiences significant diffusion, which obviously fails to represent the sharp free surface that is observed in real life. The final factor that plays a significant role locally is surface tension, which dominates in fluid breakups. In OpenFOAM® surface tension cannot be applied as a surface force due to the algebraic VOF and lack of a free surface reconstruction. Instead, surface tension is modelled approximately using the Continuum Surface Force (CSF) technique by Brackbill et al. (1992). Such method is prone to produce spurious currents and can also hinder the development of fluid breakup.

Despite all the approximations and shortcomings just outlined, which would certainly improve the simulation results if addressed/solved, we must not lose sight of the excellent agreement in pressures (Figures 6 and 7). These results were captured by gauges mounted at the cylinder face, and therefore, are heavily influenced by the local flow conditions. This means that despite not capturing water droplets or fluid breakup, the model performs adequately, this we may be able to conclude that such small details that may not play a significant role in changing pressures and forces on the cylinder significantly.

CONCLUDING REMARKS

In this paper we have analysed the interaction of two focussed wave groups impacting on a cylinder, modelled by a combination of a Lagrangian and a CFD models. The Lagrangian numerical model (Buldakov et al., 2019) has been proven to be faster than the CFD model and to produce very accurate wave kinematics in 2D, which can be used as wave generation input for the CFD model closer to the structure of interest. The one-way coupling methodology developed in Higuera et al. (2018) has been updated as part of this work. The new coupling technique allows blending the incident wave Lagrangian kinematics over a region adjacent to the wave generation boundary with a relaxation zone and is complementary to the existing BC. Both approaches appear produce equally good results, with a slight increase in computational time when applying the RZ. The model *olaFlow* is then used to simulate the detailed wave group interaction with the fixed cylinder in 3D.

Overall the degree of accordance between the experimental and numerically generated data is adequate, with mild under- or overestimations of the main wave crest and the troughs in the vicinity of the focussed group depending on the case. Generally the pressure time series shows a better agreement than FSE in both cases run. The results also indicate

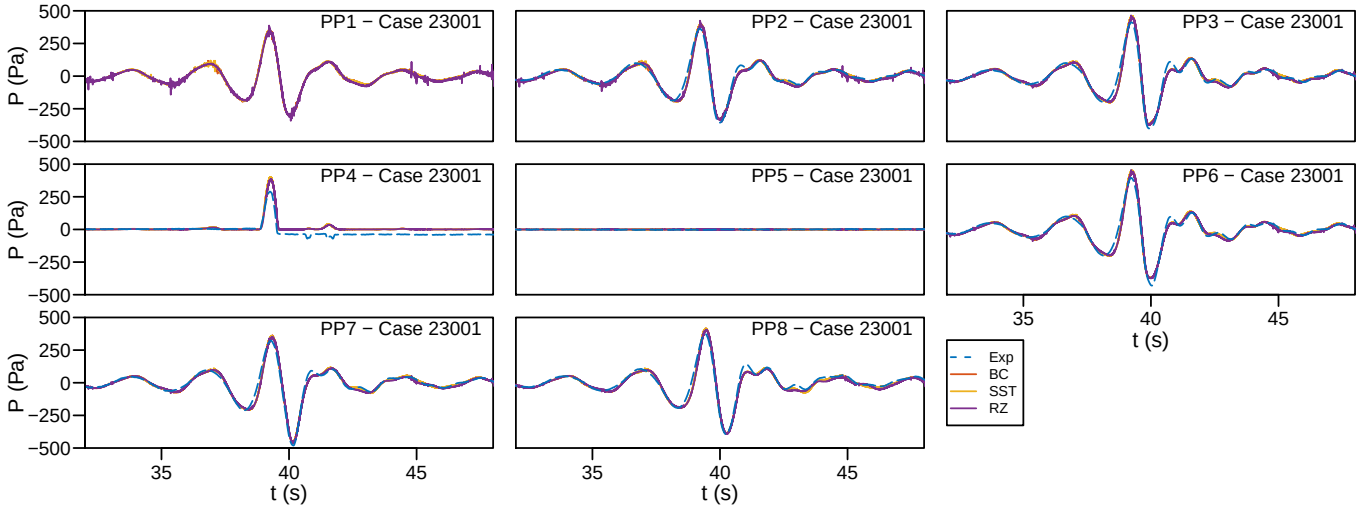

Fig. 6 Comparison of pressure time series between the experiments and the CFD simulations at gauges PP1-PP8. Case 23001.

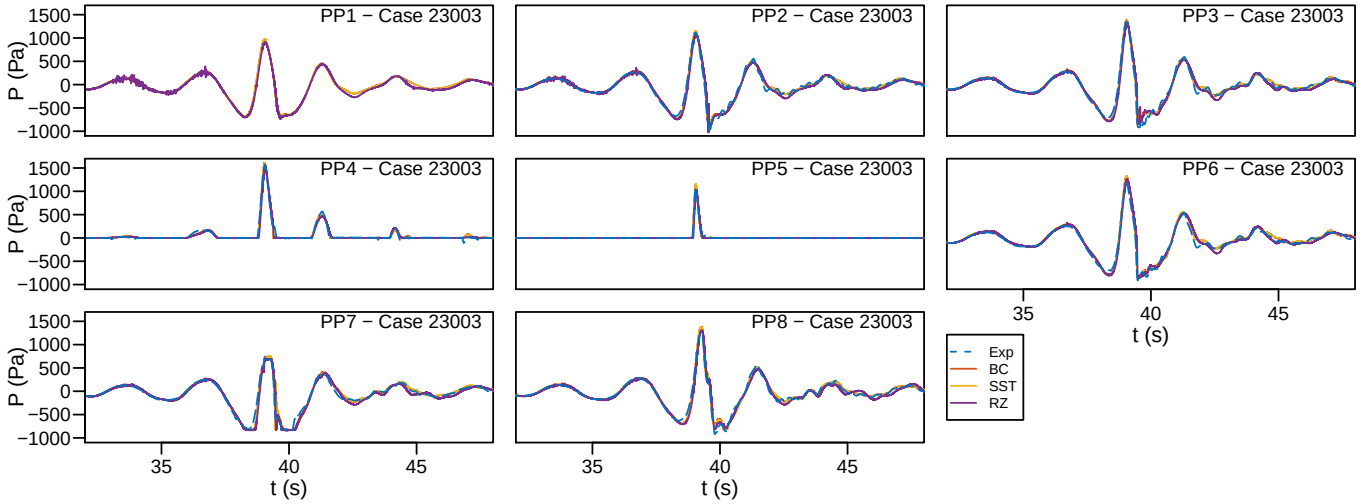

Fig. 7 Comparison of pressure time series between the experiments and the CFD simulations at gauges PP1-PP8. Case 23003.

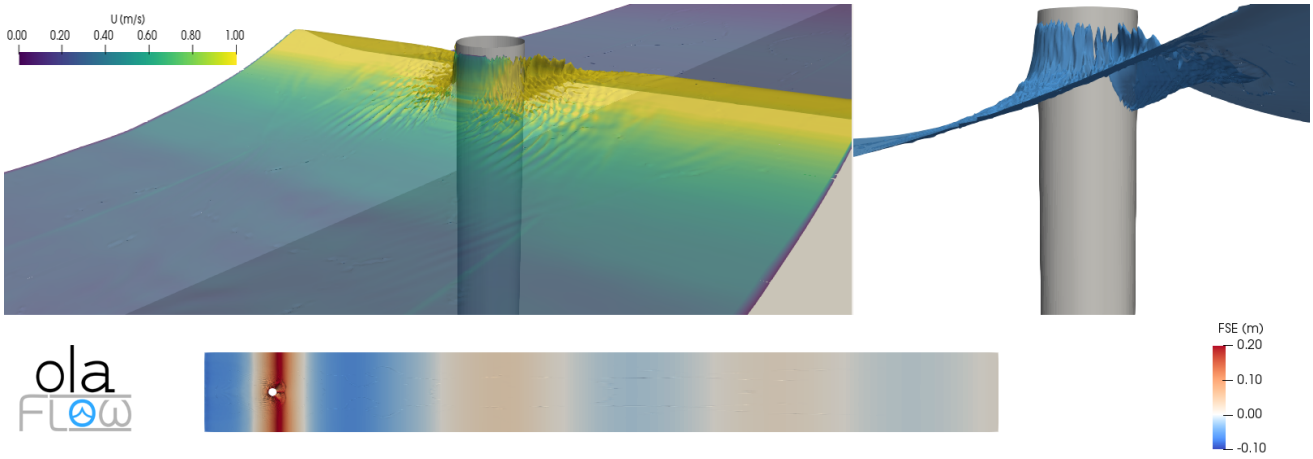

Fig. 8 Renderings of the focussed wave and cylinder interaction upon impact (t = 39 s). FSE viewed from the top (bottom panel). Flow velocities at the free surface from an isometric perspective (top left). Free surface configuration from a lateral view (top right). Case 23003.

that turbulence does not play a significant role in these particular tests, despite the violent FSE elevation gradients measured after the wave splash and runup on the cylinder. Differences between the BC and RZ wave generation approaches are also very limited.

In view of the results presented in this paper we have identified several improvements that will be performed as a future work. The RZ approach is promising in terms of enhancing wave absorption performance, especially regarding the benefits of linking it with active wave absorption. Furthermore, RZs have proven effective to generating much steeper waves than the BC method allows, thus opening a possibility to shorten the simulation domains even more by having the wave generation zone closer to the structure, i.e., closer to the focussing location where the wave group is potentially steeper. However, this implementation will require guidelines to identify its best-performing parameters, namely the relaxation zone length and the shape of the blending function, including the function itself and any parameters that it might depend on (e.g., P parameter). Another improvement to analyse would be the combined BC-RZ wave absorption efficiency to shorten the domain leeside the cylinder. This might not be so critical, because the number of cells in that area is decreasing due to the aggressive cell grading chosen (1 cm to 25 cm). Tightly linked to this, the number of spanwise cells in that area could also be reduced progressively as we move away from the cylinder and the expected 3D effects dilute. Leaving an effectively 2D flume towards the end of the CFD domain will contribute significantly to reduce the computational cost of the 3D simulations. Finally, the ultimate long-term goal of this project would be to implement a two-way coupling between the Lagrangian and *olaFlow* models, thus making concurrent runs in which incoming waves would interact nonlinearly with reflections starting from the wave generation boundary, as it occurs in the experimental facility. This approach could potentially be extended to continue with another two-way coupling after the structure, so that the complete length of the wave flume could be easily accounted for.

ACKNOWLEDGMENTS

The third author would like to acknowledge Cranfield University QR Global Challenges Research Fund (GCRF) 2019/20 for its financial contribution and support.

REFERENCES

Berberovic, E., Hinsberg, N. P. v., Jakirlic, S., Roisman, I. V., & Tropea, C. (2009). "Drop impact onto a liquid layer of finite thickness: Dynamics of the cavity evolution.". *Physical Review E*, *79*.

Brackbill, J. U., Kothe, D. B., & Zemach, C. (1992). "A continuum method for modeling surface tension.". *Journal of Computational Physics*, *100*(2), 335–354.

Buldakov, E., Higuera, P., & Stagonas, D. (2019). "Numerical models for evolution of extreme wave groups". *Applied Ocean Research*, *89*, 128–140.

Devolder, B., Rauwoens, P., & Troch, P. (2017). "Application of a buoyancy-modified k-omega SST turbulence model to simulate wave run-up around a monopile subjected to regular waves using OpenFOAM.". *Coastal Engineering*, *125*, 81–94.

Fuhrman, D. R., Madsen, P. A., & Bingham, H. B. (2006). "Numerical simulation of lowest-order short-crested wave instabilities.". *Journal of Fluid Mechanics*, *563*, 415–441.

Guo, L.-D., Sun, D.-P., & Wu, H. (2012). "A new numerical wave flume combining the 0-1 type BEM and the VOF method". *Journal of Hydrodynamics, Ser. B*, *24*(4), 506–517.

Higuera, P. (2015). *Application of computational fluid dynamics to wave action on structures*. Ph.D. thesis, University of Cantabria.

Higuera, P. (2017). "olaFlow: CFD for waves [software]". URL `https://doi.org/10.5281/zenodo.1297013`

Higuera, P. (2020). "Enhancing active wave absorption in RANS models.". *Applied Coastal Research*, *94*.

Higuera, P., Buldakov, E., & Stagonas, D. (2018). "Numerical modelling of wave interaction with an FPSO using a combination of OpenFOAM and Lagrangian models". In *Proceedings of the 28th International Ocean and Polar Engineering Conference, June 10-15 2018, Sapporo, Japan*.

Higuera, P., Lara, J. L., & Losada, I. J. (2013). "Realistic wave generation and active wave absorption for Navier–Stokes models: Application to OpenFOAM.". *Coastal Engineering*, *71*, 102–118.

Jacobsen, N. G., Fuhrman, D. R., & Fredsøe, J. (2012). "A wave generation toolbox for the open-source CFD library: OpenFOAM.". *International Journal for Numerical Methods in Fluids.*, *70*(9), 1073–1088.

Kim, S.-H., Yamashiro, M., & Yoshida, A. (2010). "A simple two-way coupling method of BEM and VOF model for random wave calculations". *Coastal Engineering*, *57*(11), 1018–1028.

Lachaume, C., Biausser, B., Grilli, S., Fraunié, P., & Guignard, S. (2003). "Modeling of breaking and post-breaking waves on slopes by coupling of BEM and VOF methods". In *Proceedings of the Thirteenth International Offshore and Polar Engineering Conference*, (pp. 1698–1704). Honolulu, Hawaii, USA.

Márquez, S. (2013). *An Extended Mixture Model for the Simultaneous Treatment of Short and Long Scale Interfaces.*. Ph.D. thesis, Universidad Nacional del Litoral.

Schäffer, H. A. (1993). "Second order irregular–wave generation in flumes-computation of transfer functions by an asymptotic summation method". In *Ocean Wave Measurement and Analysis*, (pp. 784–797). ASCE.

Skene, D. M., Bennetts, L. G., Wright, M., Meylan, M. H., & Maki, K. J. (2018). "Water wave overwash of a step". *Journal of Fluid Mechanics*, *839*, 293–312.

Sriram, V., Shagun, A., & Schlurmann, T. (2020). "Laboratory study on steep wave interaction with fixed and moving cylinder". *International Journal of Offshore and Polar Engineering*, *X*.

Weller, H., Tabor, G., Jasak, H., & Fureby, C. (1998). "A tensorial approach to computational continuum mechanics using object-oriented techniques.". *Computers in Physics*, *12*(6), 620–631.

Wroniszewski, P. A., Verschaeve, J. C., & Pedersen, G. K. (2014). "Benchmarking of navier–stokes codes for free surface simulations by means of a solitary wave". *Coastal Engineering*, *91*, 1–17.